

Results from the OPERA experiment at the CNGS beam

A Longhin on behalf of the OPERA Collaboration

via Fermi 40,00044, Frascati, Rome (IT)

E-mail: andrea.longhin@lnf.infn.it

Abstract. The OPERA experiment at the Gran Sasso underground laboratory is searching for $\nu_\mu \rightarrow \nu_\tau$ oscillations in appearance mode in the CNGS neutrino beam. Four ν_τ candidate events have been found so far, using a sub-sample of data from the 2008-2012 runs. Given the number of analysed events and the low background, $\nu_\mu \rightarrow \nu_\tau$ oscillations are established with a significance of 4.2σ . In this paper the data analysis is discussed, with emphasis on the background constraints obtained using dedicated data-driven control samples. We present also the analysis of the τ neutrino and electron neutrino data in the framework of the 3+1 sterile neutrino model. The measurement of the muon charge ratio in the collected cosmic ray sample is also reported.

1. Introduction

An increasing number of observations on neutrino oscillations has been performed since the late nineties when the phenomenon was first measured through the disappearance of atmospheric muon-neutrinos (Super-K, MACRO). A rather rich and diversified data set is well described assuming that three mass eigenstates (ν_1, ν_2, ν_3) are mixed to flavour eigenstates (ν_e, ν_μ, ν_τ) through a unitary mixing matrix (U_{PMNS} , Pontecorvo-Maki-Nakagawa-Sakata). The OPERA experiment was designed in the late nineties to unambiguously prove that the oscillation at the atmospheric scale is driven by the $\nu_\mu \rightarrow \nu_\tau$ transition. The experiment allows a direct detection of ν_τ charged-current (CC) interactions with a remarkably high signal-to-noise ratio of $\mathcal{O}(10)$.

A direct experimental evidence of neutrino appearance is a hard task which was achieved only recently in the $\nu_\mu \rightarrow \nu_\tau$ and $\nu_\mu \rightarrow \nu_e$ channels by the OPERA and T2K experiments respectively. The traditional solar and reactor neutrino sources have energy spectra well below the τ -lepton production threshold (3.5 GeV) such that both for ν_μ and ν_τ only neutral-current (NC) interactions occur. On the other hand, atmospheric or accelerator-based ν_μ sources overcome this limitation. Nevertheless the task of detecting ν_τ^{CC} interactions remains demanding due to the peculiar experimental signature of the τ -lepton which requires either a micro-metric tracking accuracy over a large volume (OPERA) or a precise characterisation of the final state kinematics with a large statistical sample. It must also be noted that the suppression of the cross section due to m_τ requires the use of relatively high beam energies, well beyond the $\nu_\mu \rightarrow \nu_\tau$ oscillation maximum, for the existing baselines of several hundreds km.

After an introduction describing the operation of the OPERA experiment (Sect. 2), the data selection (Sect. 3), the simulation (Sect. 4), the Monte Carlo validation with control data-samples, the result of the ν_τ appearance analysis is described in Sect. 5 and 6. Limits on



sterile neutrinos derived from the ν_τ search are presented in Sect. 7; in Sect. 8 we describe the measurement of $\nu_\mu \rightarrow \nu_e$. Finally in Sect. 9 the measurement of the cosmic muon charge ratio performed by OPERA at the highest energies is recalled.

2. Detector and neutrino beam

The flight length of τ leptons, for the CNGS beam has a roughly exponential distribution with a mean value of about 600 μm . The OPERA detector [1] is designed to achieve a micro-metric tracking accuracy over a very large detector volume of $(6.5 \times 6.5 \times 8) \text{ m}^3$. The target is a highly modular structure of nuclear emulsion based trackers (bricks). Bricks are interspersed with pairs of planes of horizontal and vertical scintillator strips (Target Tracker or TT) allowing to locate the target unit in which the neutrino interaction occurred with an $\mathcal{O}(\text{cm})$ resolution. A brick is composed of 57 emulsion films interleaved with 56, 1 mm thick, lead plates for a mass of 8.3 kg. Its thickness along the beam direction corresponds to about 10 radiation lengths and its transverse size is $128 \times 102 \text{ mm}^2$. A nuclear emulsion film consists of two 44 μm layers deposited on each side of a 205 μm plastic base. Changeable Sheet (CS) doublets [2, 3] are attached to the downstream face of each brick. This pair of films had received in the underground laboratory a special treatment (refreshing) to erase most of the accumulated cosmic ray background. Their scanning allows a relatively fast feedback on the prediction of the electronic detectors (ED) and provides a prediction of the event position in the brick at the $\mathcal{O}(10)\mu\text{m}$ level, thus greatly helping the vertex location. Finally a magnetic spectrometer system instrumented with Resistive Plate Chamber (RPC) detectors and high-precision Drift Tubes (DT), is used to identify muons and measure their charge and momentum. Charge determination reduces the background from charmed particles produced in charged current (CC) ν_μ interactions. The detector (Fig. 1) is divided into two identical units called Super Modules (SM), each consisting of a target and a spectrometer section. The average number of bricks has been about 140000 for a target mass of about 1.2 kt.

OPERA was exposed to the CNGS ν_μ beam [4] at a long-baseline, 730 km away from the source. The neutrino beam, produced by 400 GeV-protons accelerated in the SPS, had an average energy of about 17 GeV, optimised for the observation of ν_τ CC interactions in the OPERA detector. In terms of interactions, the $\bar{\nu}_\mu$ contamination was 2.1%, the ν_e and $\bar{\nu}_e$ contamination were together below 1%, while the intrinsic ν_τ component (from D_s decays in the CNGS target and beam-dump) was of $\mathcal{O}(10^{-6})$, hence negligible.

3. Data samples and event selection

The CNGS completed its operation on December 3, 2012. A sample corresponding to 17.97×10^{19} pot has been registered by the detector. Events are classified either as CC-like (“ 1μ ”) or NC-like (“ 0μ ”) according to data from the target tracker and the spectrometers. A 3D-track is tagged as a muon if its path length is larger than 660 g/cm². An event is classified as 1μ if either it contains at least one 3D-track tagged as a muon [5] or the total number of TT and RPC planes having at least one hit is larger than 19. The complementary sample is defined as 0μ . The 0μ sample is enriched in τ decays from $\tau \rightarrow e$, (branching ratio 17.8%), $\tau \rightarrow 1h$ (49.5%) and $\tau \rightarrow 3h$ (15.2%).

The topology and the energy deposition in the TT scintillator strips, as well as the muon track information (when available) are used to define a three-dimensional probability density map for the neutrino interaction vertex position. This probability is integrated over the volumes of the bricks and these are ranked in order of decreasing probability, for extraction and analysis.

The sample of events analyzed so far consists of the highest probability bricks, for all 0μ events and for 1μ events with a muon momentum $p_\mu < 15 \text{ GeV}/c$. In addition, for 2008-2009 CNGS runs also the second probability bricks have been analysed for all events (even those with $p_\mu > 15 \text{ GeV}/c$ which are anyway not considered in the τ analysis, as pointed out later on.)

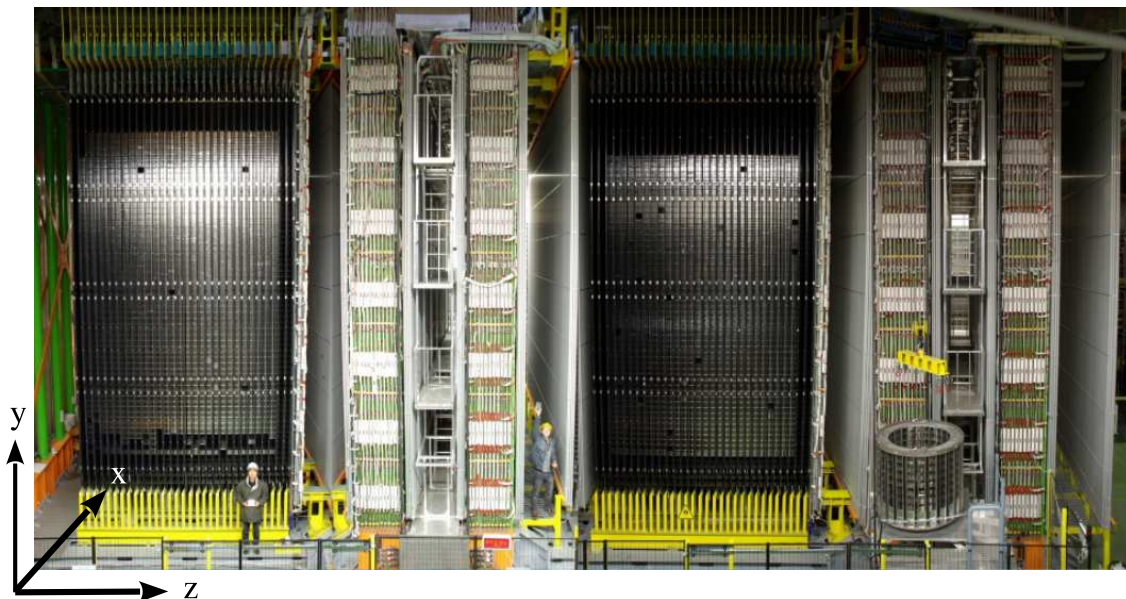


Figure 1. A picture of the OPERA detector. CNGS neutrinos travel from left to right. The (right-handed) reference frame is oriented such that: the y -axis is perpendicular to the hall floor and pointing up; the z -axis is orthogonal to the brick walls and oriented as the incoming neutrinos. The angle between the neutrino direction and the z -axis projected into the yz plane is of 58 mrad.

In the left plot of Fig. 2 the distributions of the reconstructed signed muon-momentum ($q \times p_\mu$) for 1μ -events are shown, for data and Monte Carlo (MC). The right plot in Fig. 2 shows the distributions of the brick probability for 0μ and 1μ events of the 2010 and 2011 samples, separately for the first two bricks in the probability ranking. The shape of the data is well described by the MC simulation, indicating that the event pre-selection is well understood.

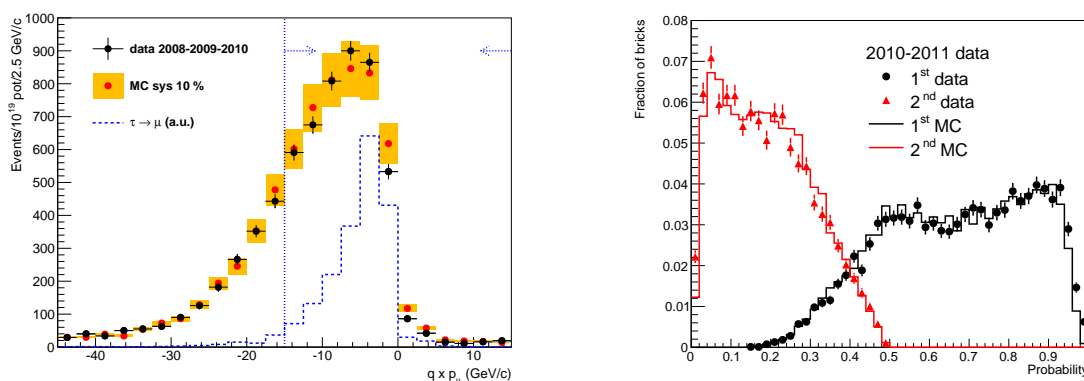


Figure 2. Left: Shape comparison of the distributions of the reconstructed muon momentum (p_μ) multiplied by the charge (q) for 1μ events for 2008-2010 data (bullets) and MC (orange band). The bar height in the MC indicates a 10% systematic error. The dashed histogram represents the $\tau \rightarrow \mu$ channel MC simulation (shape only). Right: normalised probability distributions for the 1st, 2nd brick for the data of 2010 and 2011 (bullets) and the MC (histograms). From [6].

Table 1. Summary of the analysed data samples.

year	2008	2009	2010	2011	2012	total
pot	1.74	3.53	4.09	4.75	3.86	17.97
0μ events	148	250	209	223	149	979
1μ events ($p_\mu < 15$ GeV/c)	534	1019	814	749	590	3706
all events	682	1269	1023	972	739	4685

Selected bricks were routinely extracted by a robotic Brick Manipulator System (BMS) capable of keeping up with the average weekly rate of neutrino interactions and thus allowing for the emulsion-based analysis to proceed possibly in parallel to the data taking. Removed bricks with a negative CS result are re-inserted in the target after replacement of the CS emulsion doublet. Bricks with a positive CS result are dismantled and not replaced. Empty spaces are filled by a rearrangement of bricks so to keep the target homogeneous and minimise the occurrence of events with irregularities in the energy flow containment. The time evolution of the target mass is shown in more detail in Fig. 3 (blue curve) together with the integrated number of pot (corrected for the inefficiency of the DAQ system, red curve). A 8.5% loss in target mass has been accumulated at the end of the data taking.

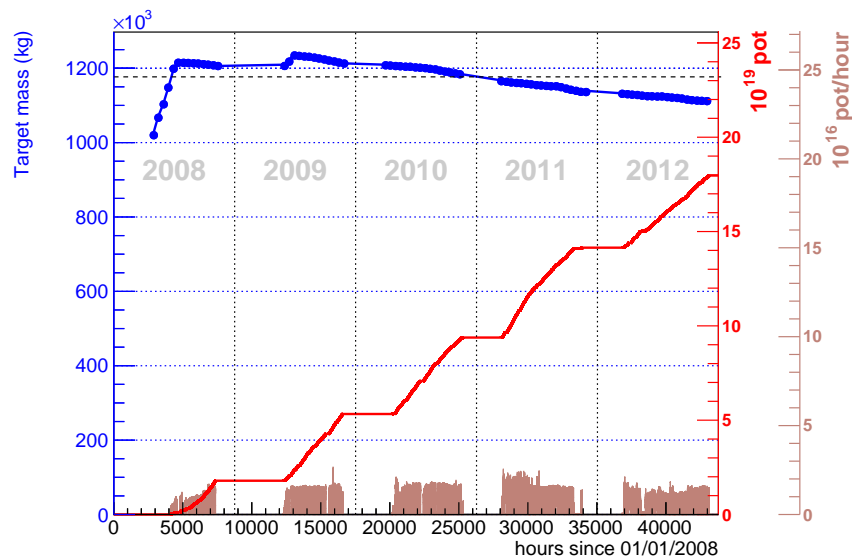


Figure 3. Evolution of the detector target mass (blue bullets) and the integrated number of pot (red line) over the whole data taking. The filled histogram shows the pot in one hour wide bins. The dashed horizontal line shows the pot-weighted average mass which amounts to 1.18 kt. From [6].

3.1. Analysis of the Changeable Sheets

Once a selected brick is extracted from the detector, the scanning of the CS doublets is performed in order to validate or disprove the brick-finding result. CS doublets can confirm the prediction of the electronic detector, or act as veto and thus trigger the extraction of neighbouring bricks. The distributions of the residuals in position and angle between the ED and CS tracks have a standard deviation of about 8 mm and 15 mrad, respectively.

In absence of a pattern of converging tracks or of a single track with a good match with the electronic-detector data, the brick is re-inserted in the target with a new CS doublet and the next brick in the probability map is extracted. In case of a positive outcome, the brick is exposed to cosmic rays in a dedicated pit in the surface LNGS laboratory for 14 hours for high-precision film-to-film alignment, later to be dismantled in the dark room where the emulsion films are developed. The films are finally dispatched to the scanning laboratories of the Collaboration for the “vertex location” and “decay search” analysis.

3.2. Vertex location in the brick

The residuals in position between the CS doublet and brick tracks are at the level of 50-60 μm such that the tracks are typically found within the predicted microscope view ($400 \times 300 \mu\text{m}$). Matching tracks are followed upstream film by film (“scan-back”) adjusting the predictions in angle and position at each step to cope with multiple Coulomb scattering (MCS) in the lead plates and measurement errors effects. If a track is not found for more than three consecutive films a volume of $1 \times 1 \text{ cm}^2$ for 5 films upstream and 10 films downstream of the stopping point is scanned and tracks within an angular acceptance $\tan \theta < 0.6$ (θ being the angle of the track with the z axis, Fig. 1) are reconstructed. In case of a shower-like topology in the CS an area of 1 cm^2 centered on the shower axis is analysed for 20 films upstream (corresponding to about $3.5 X_0$). The alignment of the films (with an accuracy of a few μm) is assured by reconstructing cosmic ray tracks.

3.3. Decay search (topological selection)

The “decay search procedure” (DS) is aimed at detecting the decay topologies of τ leptons produced in ν_τ^{CC} interactions once a vertex has been identified in the volume scan data. The decay is defined as “short” if it happens either in the same lead plate where the neutrino interaction occurred or in the first downstream emulsion layer; “long” decays are those happening further downstream such that the τ -lepton is reconstructed in at least one emulsion layer. About 54% of the τ decays are expected to be long decays. A detailed description of the decay search procedures is given in [7, 8]. The number of events with a completed decay-search for the present analysis amounts to 4685 (Tab. 1).

3.4. Kinematic selection

Several kinematic quantities of the neutrino interaction are accessible at brick-level via momentum reconstruction using MCS[9]. The energy of electrons and photons is also measured by employing calorimetric techniques [10, 11]. Kinematic criteria are defined to improve the signal-to-background ratio. To improve the acceptance for electromagnetic showers and reduce the error on the track momentum measurement the standard volume considered for the location (Sect. 3.2) is enlarged and tracks are followed downstream, eventually in other bricks (Sect. 3.5). The variables used in the kinematic selection are documented in [6]. The applied selection for each decay channel is summarised in Tab. 2. Cut parameters were studied and defined a priori in [12, 13] for the $1h$, electron and muon channels and in [14] for the $3h$ channel.

3.5. Track follow-down

The track kinematics of events fulfilling the selection are further studied in downstream bricks. Primary tracks are followed (within an angular acceptance extending up to $\tan \theta = 1$) until either a stopping point, an interaction or a muon decay topology is found (Track follow-down, TFD). Thus, by the study of momentum-range correlations, track length, energy loss in proximity of the stopping point, and (if possible) the tagging of interactions or muon decays, a muon/hadron separation exceeding the limitations of the electronic detector reconstruction is

Table 2. Kinematic selection. The meaning of the variables is defined in the text. The cut on p_T^{2ry} for the 1-prong hadronic decay is set at 0.3 GeV/c in the presence of γ particles associated to the decay vertex and to 0.6 otherwise. Cuts marked with a \star are not applied in the case of a QE event. Only long decays are considered for the $\tau \rightarrow \mu$ and $\tau \rightarrow h$ channels due to a large background component in short decays from charmed particles and hadronic re-interactions respectively.

variable	$\tau \rightarrow 1h$	$\tau \rightarrow 3h$	$\tau \rightarrow \mu$	$\tau \rightarrow e$
lepton-tag	No μ or e at the primary vertex			
z_{dec} (μm)	[44, 2600]	< 2600	[44, 2600]	< 2600
p_T^{miss} (GeV/c)	< 1 \star	< 1 \star	/	/
ϕ_{lH} (rad)	> $\pi/2\star$	> $\pi/2\star$	/	/
p_T^{2ry} (GeV/c)	> 0.6(0.3) \star	/	> 0.25	> 0.1
p_T^{2ry} (GeV/c)	> 2	> 3	> 1 and < 15	> 1 and < 15
θ_{kink} (mrad)	> 20	< 500	> 20	> 20
m, m_{min} (GeV/c ²)	/	> 0.5 and < 2	/	/

obtained. Momentum-range correlations are characterised by a discriminating variable defined as: $D_{TFD} = \frac{L}{R(p)} \frac{\langle \rho \rangle}{\rho}$ where L is the track length, $R(p)$ is the range in lead of a muon with momentum p , $\langle \rho \rangle$ is the average matter density along the path and ρ is the lead density. If $D_{TFD} > 0.8$ the track is classified as a muon track. This procedure results in all channels in a significant reduction of the background from ν_μ^{CC} charm production when the primary μ is not identified in the ED.

4. Monte Carlo simulation of signal and backgrounds

All particle trajectories are digitised at the micro-track level in a volume of $3 \times 3 \times 3$ bricks, centered on the brick containing the neutrino interaction. The efficiency and the resolution (in angle and position) of the scanning microscopes are simulated using parametrisations obtained from real data. The framework allows reproducing the analysis flow in all its steps.

4.1. Expected signal event rates

The neutrino fluxes used in the calculation of the expected signal rates are based on a FLUKA simulation of the CNGS beam-line. Neutrino interactions are generated using NEGN tuned with the parameters based on the high-statistics data sample of the NOMAD experiment[15]. The energy-dependence of the ν_τ cross section follows the default GENIE v2.6 implementation. A rate of 3.32 events/(10^{19} pot kt) is obtained assuming¹ $\Delta m_{23}^2 = 2.32 \times 10^{-3} \text{ eV}^2$ [16] and maximal mixing.

The expected number of detectable signal events in the 0μ and 1μ samples are obtained by considering the expected rates of ν_τ^{CC} and ν_μ^{CC} at “truth” level and the reconstruction efficiency for standard ν_μ^{CC} achieved for real data. Migrations of NC and CC events within the 0μ and 1μ samples are taken into account (see [6] for more details). The predictions thus obtained are insensitive to systematic effects on the efficiencies being common to ν_τ and ν_μ events. A similar approach is also used in the estimation of backgrounds.

4.2. Expected background event rates

The three main sources of background contributing to the final sample are: charmed particles decays, hadronic interactions and large-angle muon scattering (LAS).

¹ The number of oscillated events has a quadratic dependence on Δm_{23}^2 .

Table 3. Signal and background expectations for the analysed sample.

	Observed candidates	Signal events $\Delta m_{23}^2 = 2.32\text{m(eV}^2\text{)}$	All backgrounds	Charm background	LAS background	Hadronic background
$\tau \rightarrow h$	2	0.41 ± 0.08	0.033 ± 0.006	0.015 ± 0.003	/	0.018 ± 0.005
$\tau \rightarrow 3h$	1	0.57 ± 0.11	0.155 ± 0.030	0.152 ± 0.030	/	0.002 ± 0.001
$\tau \rightarrow \mu$	1	0.52 ± 0.10	0.018 ± 0.007	0.003 ± 0.001	0.014 ± 0.007	/
$\tau \rightarrow e$	0	0.62 ± 0.12	0.027 ± 0.005	0.027 ± 0.005	/	/
all	4	2.11 ± 0.42	0.233 ± 0.041	0.198 ± 0.040	0.014 ± 0.007	0.021 ± 0.006

4.2.1. Charmed particle decays. The most effective tool for the rejection of the background from charmed particles is the efficient identification of the primary muon from ν_μ^{CC} interactions. The fraction of ν_μ^{CC} events having an associated charm quark at the CNGS energies, as estimated from the CHORUS data [17], is $(\sigma(\nu_\mu^{CC} + c)/\sigma(\nu_\mu^{CC})) \otimes \phi = (4.38 \pm 0.26)\%$. In OPERA the tagging of the primary muon is achieved first, at the level of the ED, via the reconstruction of penetrating 3D-tracks and the vetoing of events involving many TT planes (to complement the tracking) as described in Sect. 3. By requiring an event to be classified as 0μ the yield is reduced down to 6% of the initial charm sample. At the emulsion detector level, a further 60% suppression is achieved applying the TFD procedure. A 20% normalisation uncertainty is assumed on this background based on the measured sample of charm events (Sect. 5.2).

4.2.2. Hadronic re-interactions. Hadronic interactions in 0μ events can mimic the topology of a single or three-prong τ decay. The kinematic selection strongly reduces this contamination due to the typical low transverse momentum of the secondary products and the reduced flight length of hadrons (the typical hadronic interaction length is much larger than the τ decay length). Further reduction is obtained by requiring the absence of nuclear fragments (either in the backward or forward hemisphere) or minimum ionising particles up to $\tan \theta = 3$. Tracks of events surviving the selection criteria have been fed to a FLUKA simulation to estimate the associated background. Several data-driven checks of this background exist based on test-beam data, the most stringent[18] being based on the analysis of a 60 m pion track length in the OPERA bricks. Hadronic nuclear fragment rates and angular distributions have also been characterised. In general a good agreement between data and simulation is observed at different pion momenta (2, 4, 10 GeV/c). Further constraints come from a sample of hadronic tracks from CNGS neutrino interactions. Present measurements allow estimating an accuracy of the predictions of the hadronic background at the 30% level. The uncertainty in the rate of high-angle nuclear fragments emitted in hadronic re-interactions is estimated at the 10% level.

4.2.3. Large-angle muon scattering. The occurrence of large-angle scattering of muons in thin ($\mathcal{O}(0.1)X_0$) lead plates is, at present, not well constrained by measurements. Upper limits from extrapolations of measurements on copper or nuclear emulsions have been reported in [12, 13]: the rates in the signal region $\theta_{kink} > 20$ mrad and $p_T^\mu > 0.25$ GeV/c for muon tracks with a realistic angular and momentum spectrum, are, at 90% C.L., $< 2.3 \times 10^{-5}$ and $< 4.1 \times 10^{-5}$, respectively. More experimental and simulation activities to determine this process are in progress. Here the same contribution used for the experiment proposal [12, 13] ($1 \times 10^{-5}/\nu_\mu^{CC}$) is assumed.

4.2.4. Summary of the expected event numbers. The estimated signal and background events for the analysed sample are summarised in Tab. 3 for each decay channel. The background from charmed particles is the dominant one in the $\tau \rightarrow e$ and $\tau \rightarrow 3h$ channels; in the $\tau \rightarrow \mu$ and in the $\tau \rightarrow 1h$ channels the largest sources of background are LAS and hadronic re-interactions,

respectively. The expected signal, considering all decay channels, amounts to $(2.11 \pm 0.42) \nu_\tau$ events. The total expected background for the sample is (0.233 ± 0.041) events.

5. Data-driven checks and control samples

5.1. Location efficiency

The dependence of the location efficiency ϵ_{loc} on E_{TT} is shown in Fig. 4 for data (2008-2009 sample) and MC, for 1μ and for 0μ events. For the 0μ sample having a large hadronic energy is important to have a good location efficiency, while, for 1μ events, efficiency at low hadronic energy can be recovered thanks to the presence of the muon track. The systematic uncertainties (bands) account for residual differences in the MC description of the data: the implementation of the CS trigger and brick scanning strategy, the definition of the dead material contribution. For the 0μ sample an additional uncertainty arises from the subtraction of the external background component. The agreement between data and MC is good in shape and normalisation for the 1μ sample while for the 0μ sample the agreement is good in shape, but data tends to be below the MC by about 15%, independently of E_{TT} . It must be noted, however, that this residual difference in the location efficiency in data and Monte Carlo for the 0μ sample has no effect on the predicted signal or background events which is normalised to the number of localised events in the data, as explained in Sect. 4.1.

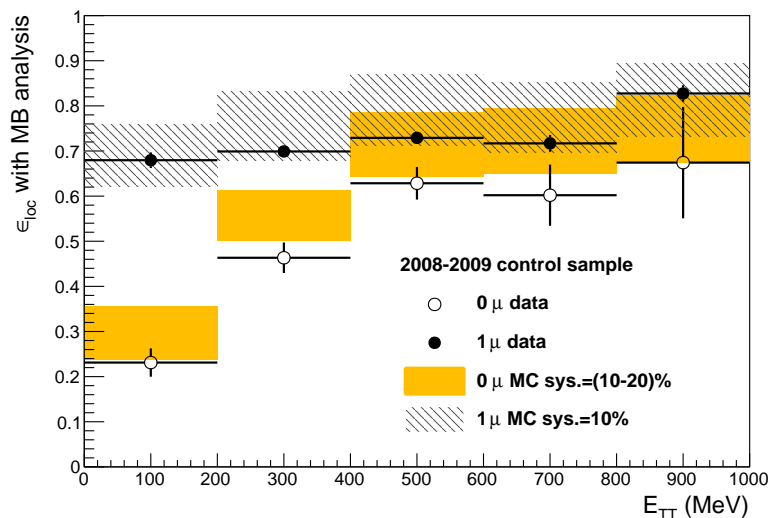


Figure 4. Location efficiency with the two-brick analysis (ϵ_{loc}) vs E_{TT} in a control sample of data collected in 2008 and 2009 (bullets) compared with MC (histograms). The comparison is done separately for 0μ and 1μ events. The error bars represent the systematical and statistical uncertainties in the MC and in the data respectively. From [6].

5.2. The charm control sample

Given the similarity in mass and decay topologies, the detection of charmed particles constitutes not only a background but also an effective tool to verify the control of the τ detection efficiency up to the topological selection (decay-search) level. An example of a CC interaction from a CNGS neutrino with an associated D^0 meson is shown in Fig. 5.

The charm yield was predicted using the latest analysis of the CHORUS data [17]. In the analysed sample of events from the 2008, 2009 and 2010 CNGS runs having at least a muon

tagged 3D-track, a total of (40 ± 3) charm events and (14 ± 3) background events are expected while 50 charm candidate events are observed in the data[8]. The distributions of the flight length of the charm candidates, the separation of the charm system and the primary muon in the beam transverse plane (ϕ), the impact parameters of the secondary particles with respect to the primary vertex and the primary muon momentum are presented in Fig. 6 for data and MC. Darker histograms represent the background due to hadronic interactions (about 87% of the total background) and decays of strange hadrons. Not only the absolute yields but also the shapes of the distributions are in very good agreement.

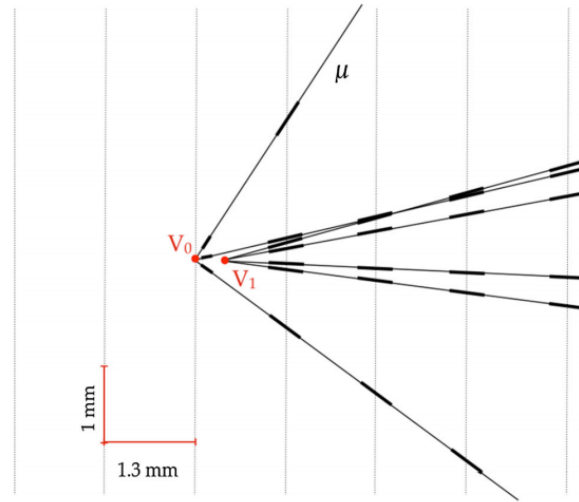


Figure 5. A reconstructed ν_μ^{CC} interaction with an associated D^0 meson. From [8].

6. Results of the ν_τ search.

The number of events in the present sample surviving the complete selection chain amounts to four τ -candidates. One of them is in the $\tau \rightarrow \mu$ decay channel[21], two in $\tau \rightarrow 1h$ ([19, 22]) and one in $\tau \rightarrow 3h$ [6]. The reconstruction in the vertex brick is shown in Fig. 7 from a lateral view. A detailed description of each candidate is reported in the references above. A summary of the kinematical properties of these events is reported in Tab. 5. Figure 4 shows the expected distribution of the scalar sum of the momenta of all particles measured in the emulsion films (p_{sum}). Red lines mark the values measured for the four candidates. In general the candidates are well inside the expected signal distributions even for other variables not shown here.

The significance of the observation of the four ν_τ candidate events is estimated by considering the confidence for excluding the null hypothesis. Two calculations based on a Fisher combination and a likelihood-ratio approach[22] yield very close results at 4.2σ . No shape information is used but just a simple counting of the observed and expected background events in each channel.

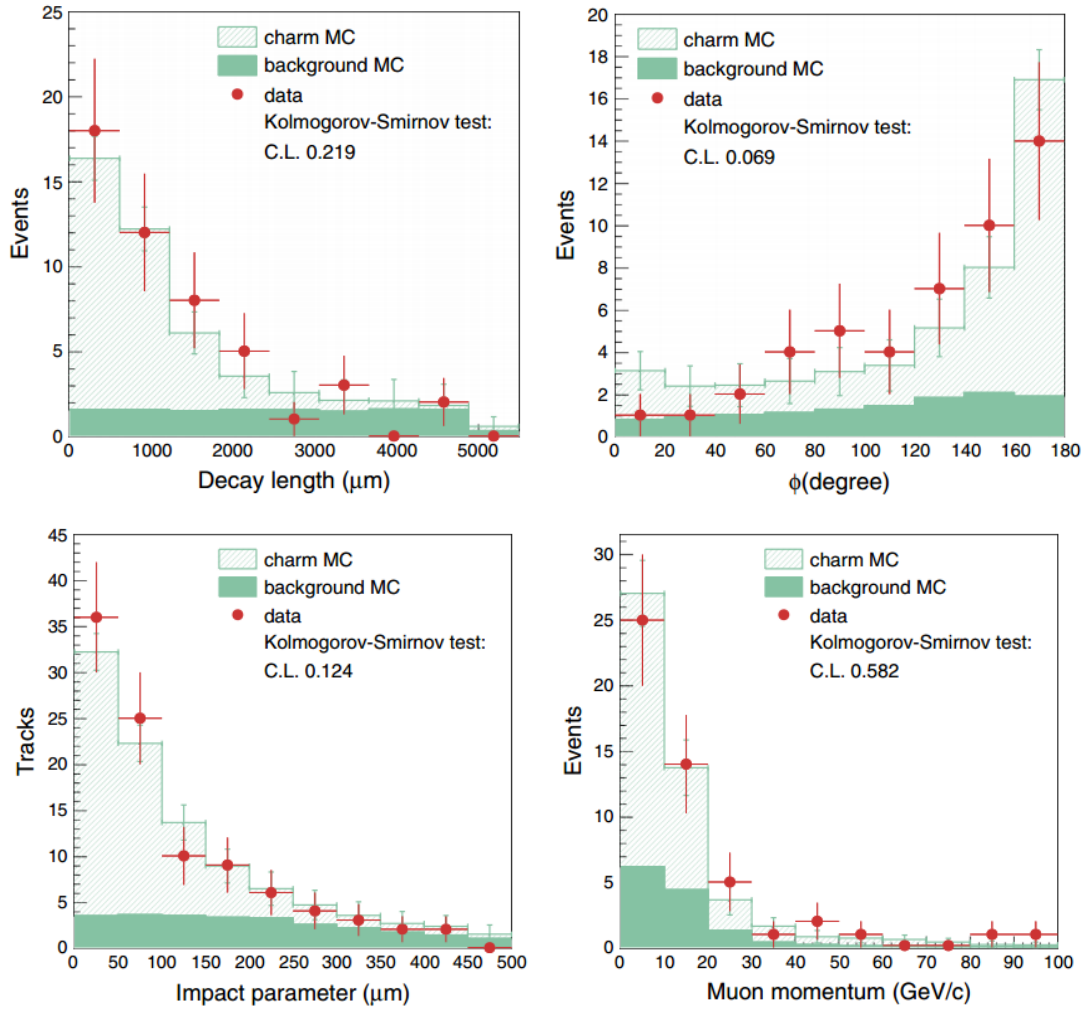


Figure 6. Shape comparison between observed ν_μ^{CC} interactions with candidate charm decays and MC expectations. Top row: (left) distribution of the decay length of the candidate charmed particles; (right) distribution of the angle between the candidate charmed particle and the primary muon in the transverse plane. The expected background contribution is also shown (stacked histogram). Bottom row: (left) distribution of the impact parameters of the candidate charm daughter particles with respect to the neutrino interaction vertex; (right) distribution of muon momentum. The expected background contribution is also shown (stacked histogram). From [8].

7. Limits on $\nu_\mu \rightarrow \nu_\tau$ oscillations induced by a sterile neutrino

Assuming the presence of an additional sterile neutrino state ν_4 the oscillation probability between ν_μ and ν_τ is modified as follows:

$$\begin{aligned}
 P(\nu_\mu \rightarrow \nu_\tau) = & 4|U_{\mu 3}^2||U_{\tau 3}^2|\sin^2 \frac{\Delta_{31}}{2} + 4|U_{\mu 4}^2||U_{\tau 4}^2|\sin^2 \frac{\Delta_{41}}{2} + 2\mathcal{R}[U_{\mu 4}^*U_{\tau 4}U_{\mu 3}U_{\tau 3}^*]\sin \Delta_{31}\sin \Delta_{41} \\
 & - 4\mathcal{I}[U_{\mu 4}^*U_{\tau 4}U_{\mu 3}U_{\tau 3}^*]\sin^2 \frac{\Delta_{31}}{2}\sin \Delta_{41} + 8\mathcal{R}[U_{\mu 4}^*U_{\tau 4}U_{\mu 3}U_{\tau 3}^*]\sin^2 \frac{\Delta_{31}}{2}\sin \frac{\Delta_{41}}{2} \\
 & + 4\mathcal{I}[U_{\mu 4}^*U_{\tau 4}U_{\mu 3}U_{\tau 3}^*]\sin \Delta_{31}\sin \frac{\Delta_{41}}{2}
 \end{aligned} \tag{1}$$

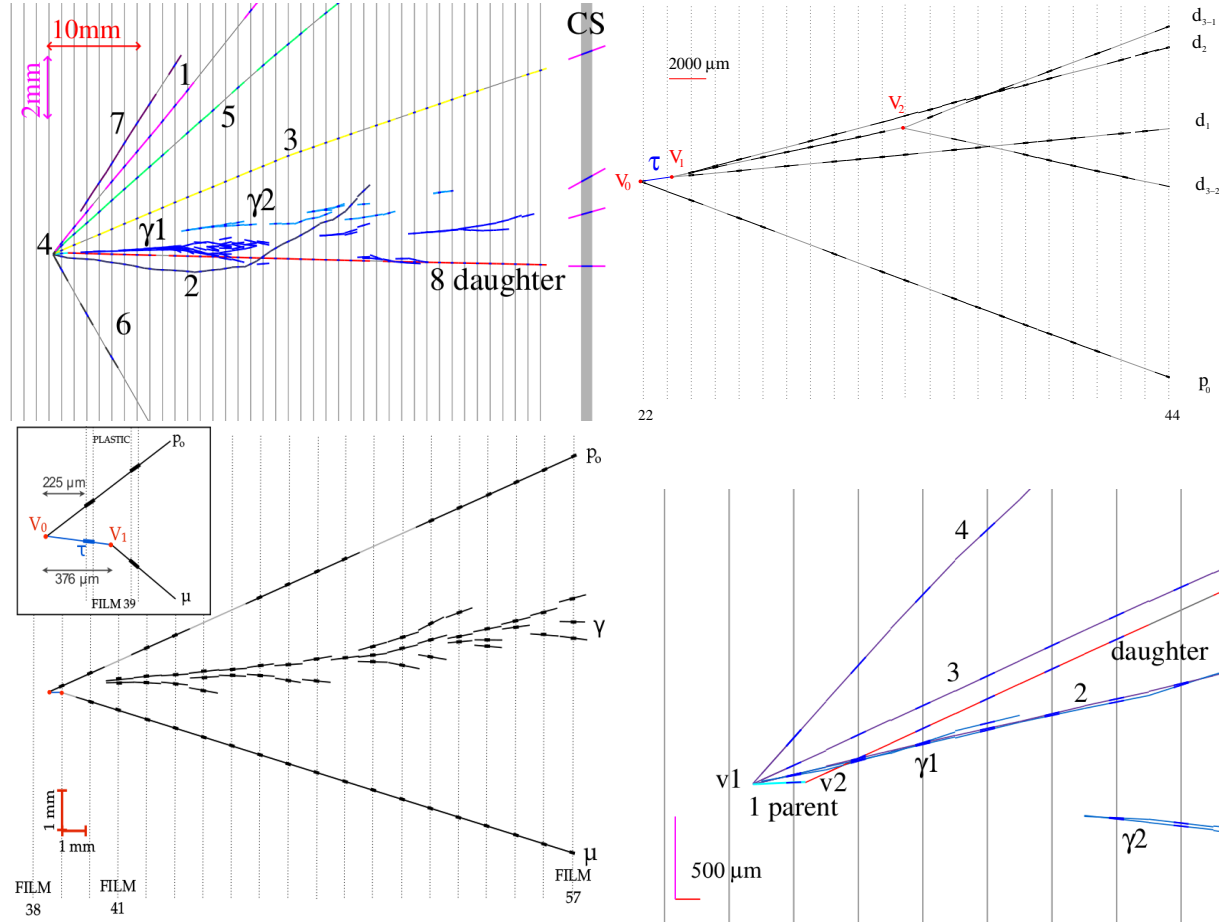


Figure 7. Event displays of the four (so far) observed ν_τ candidates: in the brick (side-view). Vertical lines indicate the position of the middle-point of emulsion films, numbering them in order of increasing z from 1 to 57. The pitch is 1.3 mm. The $\tau \rightarrow 1h$ of [19] (top left), $\tau \rightarrow 3h$ of [6] (top right), $\tau \rightarrow \mu$ of [21] (bottom left), $\tau \rightarrow 1h$ of [22] (bottom right).

where U_{ij} is an extended 4×4 PMNS matrix and $\Delta_{ij} = 1.27 \Delta m_{ij}^2 \frac{L}{E}$. Depending on the values assumed by the extra terms in the U matrix an enhancement or a suppression of the expected ν_τ can occur. The observed number of eventse was used to constrain[23] the sterile-related parameters. Figure 8, left, shows the log likelihood ratio as a function of $\sin^2 2\theta_{\mu\tau} = 2|U_{\mu 4}||U_{\tau 4}|$ for $\phi_{\mu\tau} = \text{Arg}(U_{\mu 3}U_{\tau 3}^*U_{\mu 4}^*U_{\tau 4}) = 0$ (dashed line) and after profiling the likelihood on $\phi_{\mu\tau}$ (continuous line). The right plot in the same figure shows the 90% C.L. exclusion region in the $|U_{\tau 4}|^2$ vs $|U_{\mu 4}|^2$ plane assuming $\Delta m_{41}^2 > 1 \text{ eV}^2$.

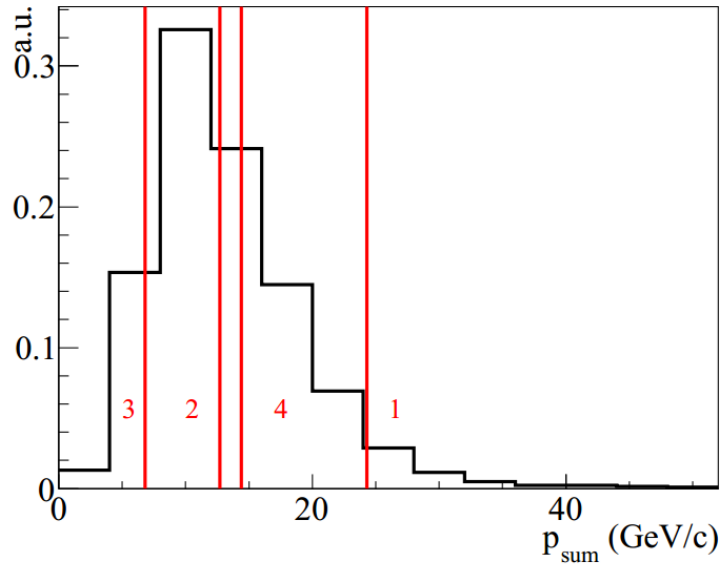
8. The $\nu_\mu \rightarrow \nu_e$ analysis

OPERA performed a measurement[11] characterising the ν_e component of the CNGS beam thanks to its remarkable electron reconstruction capabilities. Using the data from the 2008/2009 runs 19 ν_e candidates are observed with an expected background of 19.8 ± 2.8 . Figure 9, left, shows the distribution of the reconstructed energy of the 19 ν_e candidates, compared with the expected reconstructed energy spectra from the ν_e beam contamination, the oscillated ν_e from the three-flavour oscillations and the background (NC interactions with associated π^0 s and $\tau \rightarrow e$ events), normalised to the analysed pot. Below 20 GeV, 4.2 events from ν_e beam contamination

Table 4. Monte Carlo distribution of the scalar sum of the momenta of all particles (p_{sum}) measured in the emulsion films, p_{sum} , for ν_τ events passing all the cuts in all decay channels. Red lines show the measured values for the four ν_τ candidate events: 1 and 4 in the $\tau \rightarrow 1h$ decay channel, 2 in $\tau \rightarrow 3h$ and 3 in $\tau \rightarrow \mu$. From [22].

Variable	1 ($\tau \rightarrow 1h$)	2 ($\tau \rightarrow 3h$)	3 ($\tau \rightarrow \mu$)	4 ($\tau \rightarrow 1h$)
z_{dec} (μm)	435 ± 35	1446 ± 10	151 ± 10	406 ± 30
ϕ_{lH} ($^\circ$)	172.5 ± 1.7	167.8 ± 1.1	155 ± 15	166^{+2}_{-31}
$\langle \theta_{kink} \rangle$ (mrad)	41 ± 2	87.4 ± 1.5	245 ± 5	137 ± 4
p_T^{miss} (GeV/c)	$0.57^{+0.32}_{-0.17}$	0.31 ± 0.11	/	$0.55^{0.30}_{-0.16}$
p_{2ry} (GeV/c)	12^{+6}_{-3}	8.4 ± 1.7	2.8 ± 0.2	$6.0^{+2.2}_{-1.2}$
$p_{T,2ry}$ (GeV/c)	$0.47^{+0.24}_{-0.12}$	/	690 ± 50	$0.82^{+0.3}_{-0.16}$
m_{min} (GeV/c ²)	/	0.96 ± 0.13	/	/
m (GeV/c ²)	/	0.80 ± 0.12	/	/

Table 5. Selection criteria for ν_τ candidate events and corresponding measured values.



and 0.4 events from other backgrounds are expected. The expected signal from the θ_{13} driven oscillations is 1.0 event and 4 candidates are observed yielding $\sin^2(2\theta_{13}) < 0.44$ at 90% CL. The possible contribution from a sterile neutrino state has been assessed by parametrising the transition probability with an effective 2-flavour formula with an effective mixing angle. The observation translates into a 90% C.L. upper limit on $\sin^2 2\theta_{\text{eff}}$ at 7.2×10^{-3} (Fig. 9, right).

9. Measurement of the muon charge ratio

The Gran Sasso laboratory is a privileged location to study TeV-scale cosmic rays. A sample of more than 3 million charge-separated atmospheric muon events were reconstructed, among which about 110000 multiple muon bundles. The charge ratio $R_\mu = N_{\mu^+}/N_{\mu^-}$ was measured separately for single and for multiple muon events. R_μ depends on the chemical composition and energy spectrum of the primary cosmic rays, on the features of hadronic interactions, and, at high energy, on the prompt component (i.e. muons from charm decays). Hadronic interactions can be studied in the so-called “fragmentation region” in a complementary way with respect to collider experiments. Finally this observable is interesting to validate the calculations of

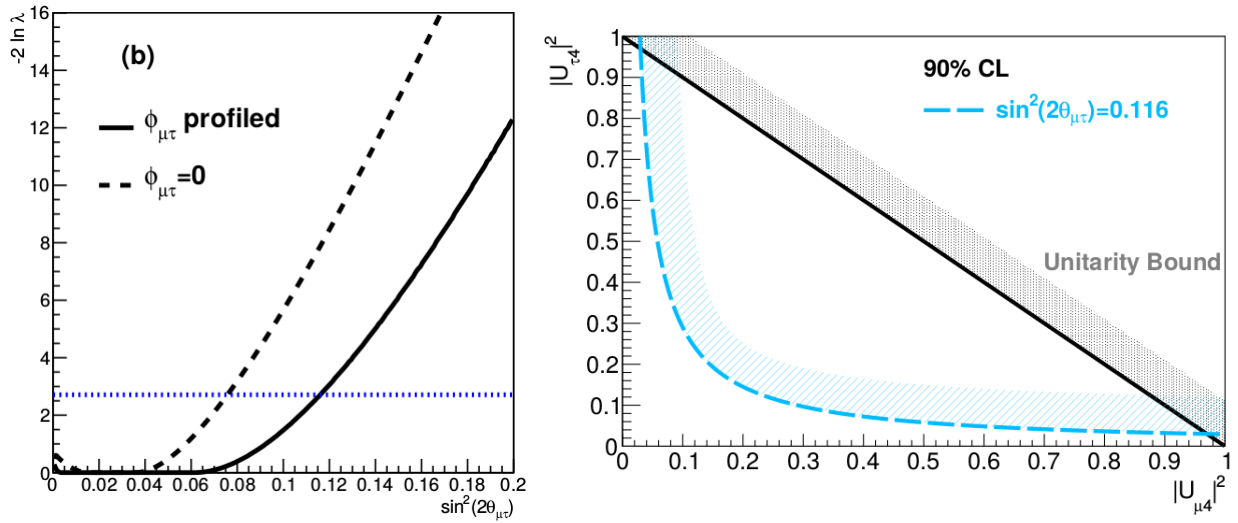


Figure 8. Left: Log likelihood ratio vs $\sin^2 2\theta_{\mu\tau}$ for $\phi_{\mu\tau} = 0$ (dashed line) and for the profile likelihood (continuous line). Right: 90% CL exclusion limits (blue line) in the $|U_{\tau 4}|^2$ vs $|U_{\mu 4}|^2$ plane assuming $\Delta m_{41}^2 > 1\text{eV}^2$. The unitarity bound (black line) is also shown. Bands are drawn to indicate the excluded regions. From [23].

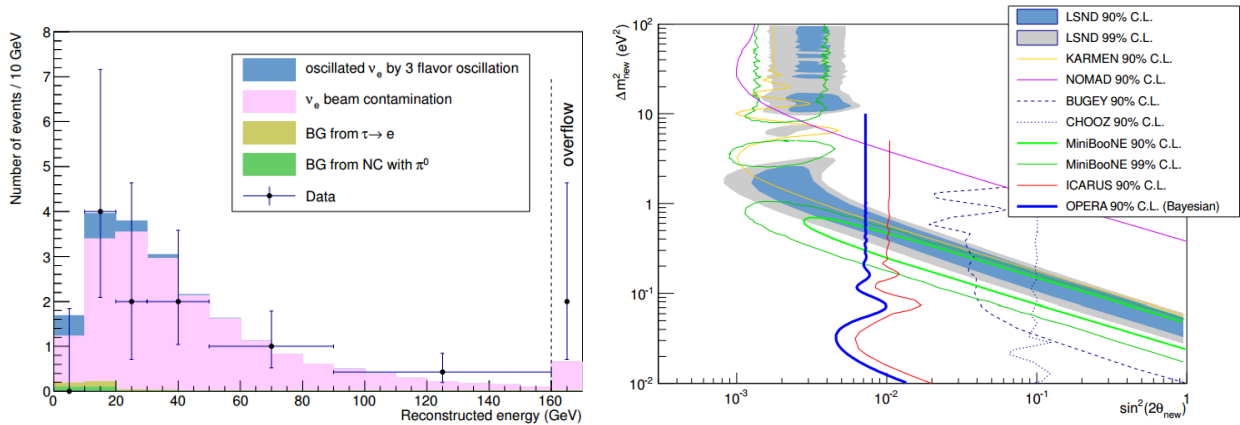


Figure 9. Left: Distribution of the reconstructed energy of the observed ν_e events; the stacked histogram shows the expected spectrum from different sources, normalised to the number of analysed pot. Right: The exclusion plot for the parameters of the non-standard $\nu_\mu \rightarrow \nu_e$ oscillation, obtained from this analysis using the Bayesian method, is shown. From [11].

atmospheric neutrino fluxes.

The analysis[24] exploited the inversion of the magnet polarity which was performed in 2012. The combination of the two data sets with opposite magnet polarities allowed minimising systematic uncertainties and reaching an accurate determination:

$$R_\mu(n_\mu = 1) = 1.377 \pm 0.006(stat.)_{-0.001}^{+0.007} \quad (2)$$

$$R_\mu(n_\mu > 1) = 1.098 \pm 0.023(stat.)_{-0.013}^{+0.015} \quad (3)$$

Data were fitted to obtain relevant parameters on the composition of primary cosmic rays and the associated kaon production in the forward fragmentation region. In the surface energy range

1-20 TeV investigated by OPERA, R_μ is well described by a parametric model including only pion and kaon contributions to the muon flux, showing no significant contribution of the prompt component (see Fig. 10). The energy independence supports the validity of Feynman scaling in the fragmentation region up to 200 TeV/nucleon primary energy. It must be noted that this measurement covers a region which had not been previously explored by any other experiment.

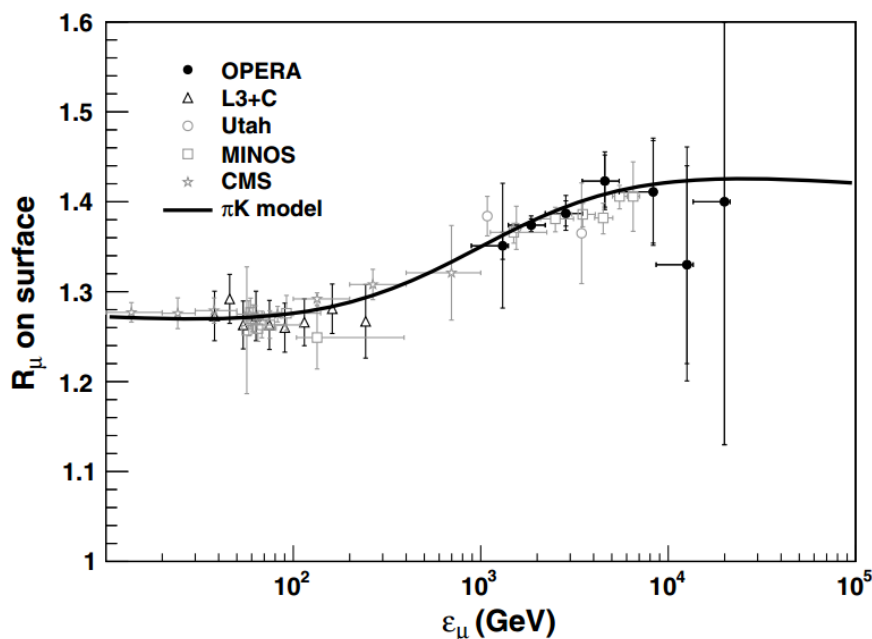


Figure 10. Measurement of the muon charge ratio as a function of the surface energy E_μ (black points). A two-dimensional fit in $(E_\mu, \cos\theta^*)$ yields a measurement of the composition parameter δ_0 (describing the proton/neutron fraction in cosmic rays nuclei) and of the Z_{pK+} moment (related to the associated production of Λ, K^+ in the forward region). The fit result is shown by the continuous line. From [24].

References

- [1] OPERA collaboration, R. Acquafredda *et al.*, *The OPERA experiment in the CERN to Gran Sasso neutrino beam*, 2009 *JINST* **4** P04018.
- [2] OPERA collaboration, A. Anokhina *et al.*, *Emulsion sheet doublets as interface trackers for the OPERA experiment*, 2008 *JINST* **3** P07005 [arXiv:0804.1985].
- [3] T. Fukuda *et al.*, *The analysis of interface emulsion detector for the OPERA experiment in JAPAN Scanning facility*, 2010 *JINST* **5** P04009.
- [4] CNGS webpage, <http://proj-cngs.web.cern.ch/proj-cngs>.
- [5] OPERA collaboration, N. Agafonova *et al.*, *Study of neutrino interactions with the electronic detectors of the OPERA experiment*, *New J. Phys.* **13** (2011) 053051.
- [6] OPERA collaboration, N. Agafonova *et al.*, *New results on $\nu_\mu \rightarrow \nu_\tau$ appearance with the OPERA experiment in the CNGS beam* *JHEP* 1311 (2013) 036, Erratum-ibid. 1404 (2014) 014.
- [7] A. Ariga *et al.*, *A method to search for short-lived particle decays in the OPERA experiment*, 2011, OPERA public note n.128. Available at <http://operaweb.lngs.infn.it/Opera/publicnotes/note128.pdf>.
- [8] N. Agafonova *et al.*, *Procedure for short-lived particle detection in the OPERA experiment and its application to charm decays*, OPERA Collaboration. *Eur. Phys. J.* **C74** (2014) 8, 2986.
- [9] OPERA collaboration, N. Agafonova *et al.*, *Momentum measurement by the multiple Coulomb scattering method in the OPERA lead-emulsion target*, *New J. Phys.* **14** (2012) 013026.
- [10] L. Arrabito *et al.*, *Electron/pion separation with an Emulsion Cloud Chamber by using a Neural Network*, *JINST* **2** (2007) P02001.

- [11] OPERA collaboration, N. Agafonova *et al.*, *Search for $\nu_\mu \rightarrow \nu_e$ oscillations with the OPERA experiment in the CNGS beam*, *JHEP* **07** (2013) 004.
- [12] OPERA collaboration, *An appearance experiment to search for $\nu_\mu \rightarrow \nu_\tau$ oscillations in the CNGS beam: experimental proposal*, *CERN-SPSC-2000-028*, (1997)
- [13] OPERA collaboration, *Status Report on the OPERA Experiment*, *CERN/SPSC 2001-025*.
- [14] A. Di Crescenzo, *Search for $\nu_\mu \rightarrow \nu_\tau$ oscillations in the OPERA experiment*, PhD thesis. Napoli Univ., April 2013. http://operaweb.lngs.infn.it/Opera/ptb/theses/theses/DiCrescenzo-Antonia_phdthesis.pdf
- [15] D. Autiero, *The OPERA event generator and the data tuning of nuclear re-interactions*, *Nucl. Phys. B (Proc. Suppl.)* **139** (2005) 253.
- [16] K. Nakamura *et al.* *Review of particle physics*, *J. Phys. G* **37** (2010) 075021.
- [17] CHORUS collaboration. A. Kayis-Topaksu *et al.* *Measurement of charm production in neutrino charged-current interactions*, *New J. Phys.* **13** (2011) 093002.
- [18] H. Ishida *et al.*, *Study of hadron interactions in a leademulsion target*, *PTEP* 2014 (2014) 9, 093C01.
- [19] OPERA collaboration, N. Agafonova *et al.*, *Observation of a first ν_τ candidate in the OPERA experiment in the CNGS beam*, *Phys. Lett. B* **691** (2010) 138 [arXiv:1006.1623].
- [20] OPERA collaboration, N. Agafonova *et al.*, *Search for $\nu_\mu \rightarrow \nu_\tau$ oscillation with the OPERA experiment in the CNGS beam*, *New J. Phys.* **14** (2012) 033017 [arXiv:1107.2594].
- [21] N. Agafonova *et al.*, *Evidence for appearance in the CNGS neutrino beam with the OPERA experiment*, *Phys. Rev. D* **89** (2014) 5, 051102.
- [22] N. Agafonova *et al.*, *Observation of τ neutrino appearance in the CNGS beam with the OPERA experiment*, OPERA Collaboration, *PTEP* 2014 (2014) 10, 101C01.
- [23] N. Agafonova *et al.* (OPERA Coll.), *Limits on muon-neutrino to tau-neutrino oscillations induced by a sterile neutrino state obtained by OPERA at the CNGS beam*, e-Print: arXiv:1503.01876.
- [24] N. Agafonova *et al.* *Measurement of the TeV atmospheric muon charge ratio with the complete OPERA data set*. *Eur. Phys. J. C* **74** (2014) 7, 2933.